

# Synthesis of ultrathin carbon films by direct current filtered cathodic vacuum arc

H.-S. Zhang and K. Komvopoulos<sup>a)</sup>

Department of Mechanical Engineering, University of California, Berkeley, California 94720

## Abstract

Direct current (dc) filtered cathodic vacuum arc (FCVA) was used to synthesize ultrathin carbon films on silicon substrates. The depth profiles, near-surface chemical composition, fractions of tetrahedral ( $sp^3$ ) and trigonal ( $sp^2$ ) carbon atom hybridizations, roughness, and hardness of the carbon films were determined from Monte Carlo (T-DYN) simulations, X-ray reflectivity (XRR), X-ray photoelectron spectroscopy (XPS), atomic force microscopy (AFM), and surface force microscopy (SFM), respectively. It was found that films with a thickness of only a few nanometers contained smaller  $sp^3$  fractions than much thicker films. The effective hardness was found to depend on the  $sp^3$  fraction and silicon-carbon composition profile. The formation of different carbon atom bonds, film growth mechanisms, and optimum process conditions for the synthesizing ultrathin carbon films are interpreted in the context of T-DYN, XRR, XPS, AFM and SFM results.

<sup>a)</sup>Corresponding Author: Tel: (510) 642-2563; Fax: (510) 643-5599; E-mail: kyriakos@me.berkeley.edu

## I. INTRODUCTION

Carbon films are used as protective overcoats in numerous industrial and scientific applications due to their high hardness and elastic modulus and excellent corrosion resistance.<sup>1-3</sup> High demand for ultrathin, durable carbon films in various leading technologies, such as hard-disk drives, dynamic microdevices, and bioimplants, has generated increased interest in deposition of ultrathin carbon films exhibiting uniformity, low roughness, high content of tetrahedral carbon atom hybridization ( $sp^3$ ), and good adhesion to substrates. Among various techniques for synthesizing carbon films, the most common are radio frequency sputtering,<sup>4-8</sup> ion-beam deposition,<sup>9-14</sup> laser ablation,<sup>15</sup> and filtered cathodic vacuum arc (FCVA).<sup>16-21</sup> FCVA is a particularly promising technique for depositing continuous, ultrathin carbon films of high  $sp^3$  contents and excellent mechanical properties.<sup>1-3,17,19,22</sup> For example, hydrogen-free carbon films synthesized by FCVA have been reported to exhibit hardness approaching that of diamond.<sup>21,23,24</sup>

Significant efforts have been devoted to improve the FCVA technique by analyzing the discharge mechanisms,<sup>2,24-26</sup> improving macroparticle filtering,<sup>16,27-29</sup> and using pulsed or direct current (dc) arc.<sup>18,19,25,30</sup> However, the limiting carbon film thickness and associated FCVA conditions have not been determined yet. For film thickness of only a few nanometers, compositional variations could be significant due to the effect of interfaces. Ion implantation simulations have been proven powerful tools for determining stoichiometric distributions. Important insight has been gained from calculations of energetic atom displacements in solids and simulations of ion trajectories.<sup>31-36</sup> The TRIM code, one of the most common Monte Carlo ion trajectory simulation program, which initially accounted only for ion interactions with the virgin target,<sup>37</sup> was modified to include the effects of ion backscattering, re-sputtering, target atom displacement, and phonon/electron excitations, enabling dynamic simulations involving ion

cascades and continuously changing composition.<sup>38,39</sup> T-DYN is a dynamic simulation code based on TRIM, which has been verified by experimental results of atomic mixing,<sup>40</sup> depth profile,<sup>9,10,41</sup> and sputtering yield.<sup>42,43</sup>

Earlier studies have revealed a correlation between high hardness and high  $sp^3$  content of carbon films.<sup>1,2,19,21,23</sup> Hard carbon films with high  $sp^3$  contents have been synthesized under a carbon ion energy of  $\sim 120$  eV, corresponding to  $-100$  V pulsed substrate bias voltage and  $\sim 20$  eV initial carbon ion energy of the cathodic arc discharge.<sup>2,19,21,44,45</sup> One of the main objectives in this study was to determine if the good properties of films synthesized under  $\sim 120$  eV carbon ion energy can be preserved while decreasing the process time, which is linearly related to the ion fluence, to obtain uniform carbon films of minimum thickness. The FCVA conditions corresponding to the ultrathin film region were studied by fixing the process time and tuning the substrate bias. X-ray photoelectron spectroscopy (XPS) was used to systematically examine carbon bonding changes in terms of implanting ion fluences and substrate bias. Film thickness and composition depth profiles were determined from T-DYN simulations and X-ray reflectivity (XRR) measurements. The film roughness, measured with an atomic force microscope (AFM), was interpreted in terms of atomic carbon bonding and carbon atom diffusion at the film surface. The nanomechanical properties of the films were investigated with a surface force microscope (SFM). The results provide insight into the carbon bonding formation and growth mechanisms of ultrathin carbon films synthesized by the FCVA method.

## **II. EXPERIMENTAL PROCEDURES**

### **A. Synthesis of carbon films by FCVA**

Synthesis of carbon films on Si(100) substrates was accomplished with a custom-made dc FCVA system by applying constant potential and current between the anode and cathode of 24 V and 70 A, respectively. A detailed description of this system is given elsewhere.<sup>46</sup> Although the dc arc discharge yields high deposition rates, it is limited by arc discharge instabilities. In the current system, a special design of the magnetic field at the cathode and the anode was used to stabilize the arc discharge.<sup>46</sup> It was found that carbon ions arrived at the substrate surface at a flux rate of  $\sim 1.48 \times 10^{15}$  ions/cm<sup>2</sup>·s. Macroparticle filtering was achieved with an out-of-plane S-configuration magnetic filter. The substrate was pulsed biased at a frequency of 25 kHz with a voltage of average value varying from 0 to  $-300$  V. All of the FCVA experiments were performed on 4-inch-diameter Si(100) wafers which were first sputter-cleaned for 3 min with a 500-eV, 16-mA Ar<sup>+</sup> ion beam at 60° incidence angle. During sputter cleaning and FCVA processing, the substrate holder was rotated at 60 rpm to obtain an etched layer and a carbon film of uniform thickness. A cryogenic pump was used to obtain a base pressure of less than  $3 \times 10^{-7}$  Torr in all film syntheses.

### **B. Thickness and compositional profiles**

The binary atom collisions during the FCVA process were simulated by classical-trajectory method using the T-DYN software (version 4.0) to give the composition profiles. The ion energy and ion fluence, measured experimentally, were the input parameters in the T-DYN simulations, performed to a depth of 20 nm from the top surface layer in 100 evenly split channels. Details of the conditions and logarithms are given elsewhere.<sup>40</sup> The binding energy for Si and C were set to 2.32 and 2.27 eV, respectively, and the corresponding surface binding

energies to 4.7 and 7.41 eV, respectively. These are standard values for solid-state silicon and graphite. The impinging ion energy was set equal to the summation of the initial carbon ion energy of 20 eV (statistically, the most likely value<sup>45</sup>) and the energy due to the substrate biasing (in the range of 0–300 eV). All ions were assumed to impinge the substrate surface in the normal direction.

Film thickness measurements were obtained by XRR using a commercially available set up (X'Pert PRO MRD, PANalytical, The Netherlands) with an X-ray wavelength of 0.154052 nm produced by a Cu-K $\alpha$  X-ray tube. The generator current and voltage were set at 40 mA and 45 kV, respectively, the step size at 0.005 $^\circ$ , and the step time at 0.5 s.

### **C. Microstructure analysis**

The synthesized carbon films were characterized by an XPS system (PHI 5400, Physical Electronics) equipped with a monochromatic X-ray source of Al-K $\alpha$  (1486.6 eV). XPS was chosen because it can provide quantitative information about the bonding energy and bonding percentage of linear ( $sp^1$ ), trigonal ( $sp^2$ ), and tetrahedral ( $sp^3$ ) carbon hybridizations, and high-energy contamination bondings.<sup>8</sup> In the case of ultrathin films, bonding of the film to the substrate and ambient adsorbents cannot be neglected. In addition, XPS has a detection depth of ~10 nm and, therefore, is suitable for surveying the overall bonding state of films with thickness less than 10 nm. The spectrometer was operated at pass energy of 35.75 eV for the C1s window scan. A 0.05-eV energy step applied in 50 ms increments was used to acquire the XPS spectra of the C1s peak. The area resolution of the XPS analyzer was ~1 mm<sup>2</sup>. The pressure in the XPS analyzing vacuum chamber was less than  $2 \times 10^{-8}$  Torr. The samples were not sputter cleaned before the XPS analysis.

The root-mean-square (RMS) surface roughness of the carbon films was measured with an AFM (Dimension 3100, Veeco Digital Instruments) using  $1 \times 1 \mu\text{m}^2$  scan areas. The AFM was operated in the tapping mode, using a drive frequency of 259.332 kHz and scan rate of 2 Hz.

#### **D. Nanomechanical testing**

The surface nanomechanical properties of the carbon films were studied with a SFM consisting of an AFM (Nanoscope II, Digital Instruments) retrofitted with a force transducer (Hysitron, Minneapolis, MN) having a sharp diamond tip of radius of  $\sim 67$  nm. Details of the SFM system can be found elsewhere.<sup>47</sup> The tip area function versus indentation depth was obtained from a calibration with a standard fused quartz with in-plane modulus equal to 69.6 GPa. The triangular loading function with both loading and unloading times equal to 2 s was used in all nanoindentations. The hardness was measured as the ratio of the maximum load to the projected contact area of the diamond tip at the corresponding indentation depth.

### **III. RESULTS AND DISCUSSION**

#### **A. Film thickness and composition profiles**

In earlier studies it was observed that the highest  $sp^3$  content and best mechanical properties of relatively thick carbon films corresponded to a carbon ion energy of  $\sim 120$  eV.<sup>2,19,21,44</sup> Therefore, T-DYN simulations were first performed for carbon ion energy of 120 eV. Figure 1 shows carbon depth profiles in silicon for carbon ion fluence in the range of  $0.1\text{--}9.0 \times 10^{16}$  ions/cm<sup>2</sup>. While the increase of the ion fluence enhances the near-surface carbon concentration, it causes the carbon profile to extend deep into the silicon substrate. For low ion fluence ( $< 1.0 \times 10^{16}$  ions/cm<sup>2</sup>), the maximum carbon concentration occurs at a distance of  $\sim 1.5$  nm below the surface, which is the average stopping range of 120-eV carbon ions in silicon. An atomic fraction of carbon of  $\sim 80$  at% is reached at the surface for a fluence of  $1.8 \times 10^{16}$  ions/cm<sup>2</sup>,

which causes the carbon profile to extend to a depth of ~6 nm. To obtain a uniform, high carbon concentration (~90 at%) up to a depth of ~10 nm the ion fluence must be increased above  $6.3 \times 10^{16}$  ions/cm<sup>2</sup>. The compositional gradients in the depth profiles suggest that prescribing a unique film thickness for a given ion fluence is subjective. Therefore, it is preferred to use the composition profile for each FCVA process rather than the film thickness.

Figure 2 shows T-DYN simulation results revealing the effect of carbon ion energy (or substrate bias) under fixed ion fluences on the carbon depth profile. The ion fluences of 3.6 and  $1.8 \times 10^{16}$  ions/cm<sup>2</sup> correspond to process times of 0.4 and 0.2 min, respectively. A comparison of Figs. 2(a) and 2(b) indicates that the surface carbon concentration increases with ion fluence and decreases with the increase of the ion kinetic energy, while the thickness of the carbon-modified surface layer increases with the ion kinetic energy and ion fluence. The shallowest carbon profile (~5 nm) of high surface carbon content (~95%) is achieved for ~20 eV ion kinetic energy and  $1.8 \times 10^{16}$  ions/cm<sup>2</sup> ion fluence, i.e., 0.2 min process time without substrate bias [Fig. 2(b)]. High ion energy enhances the implantation range of carbon ions, resulting in the broadening of the carbon depth profile. Therefore, low ion kinetic energy is needed to synthesize a carbon (~95 at% C) film of minimum thickness (~2 nm).

Because in the T-DYN simulations a uniform ion impinging energy was assumed and chemical reactions, diffusion, and atomic bond formation were neglected, the simulation results are applicable for low ion fluences under which the previous mechanisms can be neglected as producing insignificant localized effects on the composition. XRR measurements were used to validate the T-DYN results. The intensity of the reflected X-ray depends on the surface and near-surface electron density.<sup>48</sup> The depth where the carbon fraction decreases sharply controls the intensity of the reflected X-ray. Figure 3 shows XRR curves for ~120 eV ion kinetic energy, i.e.,

–100 V pulsed substrate bias. The periodic fringe patterns can be related to the X-ray travel length through the sample surface.<sup>49,50</sup> By performing a fast Fourier transform of the periodic curves,<sup>51,52</sup> the calculated depth of the X-ray reflection was found equal to 40.2, 27.1, 12.5, 6.7, and 2.3 nm for process time equal to 3.0, 1.5, 0.7, 0.4, and 0.2 min, respectively. The 2.3, 6.7, and 12.5 nm depth values are close to the shoulder edge of the T-DYN simulation profiles for ion fluence equal to 1.8, 3.6, and  $6.3 \times 10^{16}$  ions/cm<sup>2</sup> (Fig. 1). The critical angle in the XRR curves was found to decrease with the ion fluence, suggesting a decrease in the density of the surface layer.<sup>49</sup> However, density calculations based on the critical angle were avoided due to the absence of a uniform composition profile.

## **B. Microstructure and associated mechanisms**

Figure 4 shows a deconvoluted XPS C1s peak corresponding to ~170 eV ion kinetic energy (–150 V pulsed substrate bias voltage of 25 kHz frequency) and 0.4 min process time, which is representative of the C1s peaks obtained from most FCVA experiments. Six Gaussian profiles with characteristic binding energies were fitted to the C1s peak after performing the Shirley inelastic background subtraction,<sup>53</sup> and each profile was associated with a carbon constituent of a certain chemical state. Details of the deconvolution and interpretation of each profile can be found elsewhere.<sup>8</sup> Peaks C1s-1, C1s-2, and C1s-3 correspond to  $sp^1$ -,  $sp^2$ - and  $sp^3$ -coordinated carbon hybridizations, respectively, while peaks C1s-4, C1s-5, and C1s-6 correspond to carbon bonding to the surface adsorbants<sup>4,8</sup> and, hereafter, will be referred to as satellite peaks. The sum of the satellite peak areas indicates the percentage of surface-adsorbent-related carbon bonding. The respective fraction of each bonding can be estimated by calculating the area of the corresponding peak, as proposed in previous studies.<sup>54,55</sup> The formation of  $sp^3$  hybridizations in carbon films has been attributed to various mechanisms explained by different

models, such as subplantation,<sup>1,2,9,11</sup> carbon-carbon atomic probabilistic collision,<sup>7</sup> and compressive stress.<sup>56,57</sup> However, these mechanisms are applicable for relatively thick carbon films synthesized under high ion fluence conditions.

A dramatic change in carbon hybridization was observed with the decrease of the ion fluence. For an ion kinetic energy of  $\sim 120$  eV, the binding energies corresponding to  $sp^1$ ,  $sp^2$ , and  $sp^3$  hybridizations exhibited marginal changes with the variation of the process time, except for very short process times, i.e., very shallow depth profiles [Fig. 5(a)]. The higher binding energies obtained for relatively short process times (i.e.,  $< 0.5$  min) correlate with a significant change in  $sp^2$  and  $sp^3$  hybridizations [Fig. 5(b)]. This result is in qualitative agreement with the reported low  $sp^3$  fraction of thin carbon films.<sup>20</sup> According to the subplantation model,<sup>9-11</sup> energetic carbon ions penetrate into the substrate up to some depth, and the resulting carbon densification in the subsurface leads to a higher  $sp^3$  content compared to that in the near-surface region ( $< 1.5$  nm). Thus, the enhancement of  $sp^3$  hybridization is driven by a subsurface mechanism that requires a minimum thickness of high carbon concentration of  $\sim 1.5$  nm. Another plausible explanation is the presence of a tensile stress in the tail of the carbon profile, as proposed for carbon/silicon interfaces where carbon atom bonding to the silicon surface gives rise to a tensile stress.<sup>5</sup> Although this tensile stress can be relaxed by diffusion, a low  $sp^3$  fraction is not favored in the carbon-silicon interfacial layer.

Low-ion-fluence FCVA was further studied with XPS by varying the substrate bias. Figure 6 shows the variation of different carbon bonding with the substrate bias for short process times. As mentioned earlier, the satellite fractions are related to physical adsorption of airborne contaminants, depending on the film microstructure and surface carbon bonding, i.e., unstable carbon at the surface may easily react with ambient contaminants. These reactions can cause a

decrease in the  $sp^3$  content.<sup>58</sup> The highest  $sp^3$  content (~45%) was obtained with -150 V substrate bias voltage for process time fixed at 0.4 min [Fig. 6(a)]. The decrease of the process time to 0.2 min to obtain a shallower carbon profile necessitated a bias voltage of -50 V to yield maximum  $sp^3$  content of ~40% [Fig. 6(b)]; however, these FCVA process conditions do not appear to be as conducive to  $sp^3$  formation as those of the previous case. According to the subplantation model, low-energy ions penetrating into the substrate induce a compressive stress and promote  $sp^3$  hybridization.<sup>9,11</sup> Any excess of ion energy can cause stress relaxation, atomic diffusion, and decrease in  $sp^3$  bond formation.<sup>6,44</sup> The high  $sp^1$  and low  $sp^2$  contents obtained under a substrate bias voltage of -300 V can be attributed to chemical reaction of C with Si. X-ray diffraction has revealed the formation of nanocrystalline SiC at the carbon-silicon interface.<sup>46</sup> When carbon is bonded with silicon, a significant  $sp^1$  peak (C1s-1 position) has been observed in the deconvoluted XPS C1s peak.<sup>59-61</sup> It is likely that for an average ion kinetic energy of ~320 eV, a significant portion of the ion energy distribution is above the activation energy of SiC and, therefore, the  $sp^1$  hybridization is related to both carbon-carbon and carbon-silicon linear bonding.

The roughness data shown in Fig. 7 provide information for the initial stage of surface modification and additional evidence of  $sp^3$  formation. In general, lower  $sp^3$  content is accompanied by higher surface roughness.<sup>11</sup> However, for ultrathin films the surface roughness is controlled by the silicon substrate.<sup>62</sup> In Fig. 7(a), the data point at zero process time corresponds to the  $Ar^+$  sputter-cleaned silicon substrate. Carbon atom adsorption and bonding at the sputter-roughened silicon surface is a spontaneous and highly exothermic process,<sup>63</sup> presumably resulting in the decrease of the initial roughness. The process time of 0.7 min may correspond to the transition from relatively low to high carbon concentration profile and the

greatest effect of surface smoothening by carbon atom adsorption. The roughness values for longer process time correspond to carbon profiles with increased  $sp^3$  contents. The decrease of the surface roughness with the increase of the process time may be related to the increase of the ion fluence, which promoted surface smoothening through the increase of the amount of carbon delivered to the surface. The low surface roughness for 0 and  $-50$  V bias voltage shown in Fig. 7(b) for fixed ion fluence may be attributed to a greater affinity of carbon atoms to adsorb and diffuse at the substrate surface, resulting in a smoothening effect. A local roughness peak is reached at a  $-100$  V bias voltage due to deeper ion penetration and less carbon species at the surface resulting from the higher ion energy. The decrease in surface roughness for bias voltage between  $-100$  and  $-200$  V can be associated with the lower  $sp^3$  content of the film profiles causing a slight increase in resputtering and surface smoothening by low-degree surface diffusion. The significant roughening caused for bias voltage above  $-200$  V is due to the intense bombardment of carbon ions that induced excessive atomic diffusion and surface damage.<sup>6,9,11,44</sup>

### **C. Nanomechanical behavior**

Figure 8(a) shows a representative nanoindentation response for a sample processed at  $\sim 120$  eV ion kinetic energy and 3 min process time. The small residual displacement after unloading and force hysteresis defined by the loading and unloading paths of the nanoindentation response illustrates the resistance of the surface to plastic deformation. The significantly larger force hysteresis obtained with the original silicon substrate demonstrated the marked enhancement of the surface resistance to plastic deformation due to the formation of the carbon film. Using such force versus displacement curves, the maximum contact pressure was calculated by dividing the maximum indentation load by the projected area, determined from the tip shape function at the maximum displacement. Figure 8(b) shows that the variation of the maximum

pressure with the maximum displacement comprises two regions. In the first region, the contact pressure increases as plastic deformation accumulates below the tip. The decrease of the contact pressure in the second region is due to the more pronounced substrate effect at larger indentation depths. The peak of the maximum contact pressure represents the effective hardness of the processed material. The term effective hardness is used because it is a function of both the carbon film and substrate properties and reflects the surface resistance against plastic flow.<sup>21,23,47,50</sup> The dependence of the effective hardness on process time and substrate bias is shown in Fig. 9. For fixed ion kinetic energy ( $\sim 120$  eV), the effective hardness increased with the process time [Fig. 9(a)]. This trend can be mostly attributed to the substrate effect, which becomes more significant with thinner films. For process time of 0.2 and 0.4 min, the highest effective hardness is obtained for bias voltage between  $-50$  and  $-100$  V [Fig. 9(b)]; however, higher effective hardness values were produced for 0.4 than 0.2 min process time due to the substrate effect. In addition to the substrate effect, the  $sp^3$  carbon hybridization may also affect the nanomechanical properties. For fixed carbon ion fluence,  $sp^3$  fraction was found to correlate to the effective hardness (Figs. 6 and Fig. 9). While high  $sp^3$  fraction results in high effective hardness, low carbon concentration due to deep penetration of high-energy carbon ions decreases the effective hardness. The trends shown in Fig. 9(b) are manifestations of two competing effects, namely  $sp^3$  carbon hybridization and carbon-silicon intermixing.

#### IV. CONCLUSIONS

Ultrathin carbon films were synthesized onto silicon substrates using the FCVA technique. Carbon films with different compositions, roughness, and nanomechanical behaviors were obtained by varying the carbon ion kinetic energy (substrate bias) and ion fluence (process time). The carbon film profiles were simulated with the T-DYN code and validated by XRR

measurements. Results from XPS, AFM, and SFM analyses yielded insight into the microstructure, roughness, and nanohardness characteristics of the synthesized carbon films and mechanisms of carbon atom hybridization. Carbon films synthesized without substrate bias (~20 eV ion energy) produced high carbon concentrations at the surface but relatively low  $sp^3$  contents, while high ion kinetic energies (>200 eV) degraded the film strength and increased the surface roughness. In the case of ultrathin films (<5 nm), i.e., 0.4 and 0.2 min process time, the highest  $sp^3$  content was obtained for substrate bias voltage of -150 and -50 V, respectively. The surface roughness was found to depend on the surface carbon concentration, and was also influenced by two competing mechanisms – surface diffusion that induced surface smoothing and intense ion bombardment that caused surface damage. The effective hardness for relatively short process time (i.e., 0.2 and 0.4 min) was influenced by the substrate deformation,  $sp^3$  fraction, and carbon concentration in the film.

## **ACKNOWLEDGMENTS**

This research was funded by the Information Storage Industry Consortium (INSIC), Extremely High Density Recording (EHDR) Program, and the Computer Mechanics Laboratory (CML), University of California, Berkeley. The authors acknowledge Professor R. Ramesh and his graduate student L. Martin for the XRR experiments, Professor Y. Suzuki for the use of the AFM, and Dr. A. Anders for helpful discussions on FCVA.

## REFERENCES

- <sup>1</sup>J. Robertson, Mater, Sci. Eng., R. **37**, 129 (2002).
- <sup>2</sup>J. Robertson, Thin Solid Films **383**, 81(2001).
- <sup>3</sup>T. Yamamoto and H. Hyodo, Tribol. Inter. **36**,483 (2003).
- <sup>4</sup>W. Lu, K. Komvopoulos, and S. W. Yeh, J. Appl. Phys. **89**, 2422 (2001).
- <sup>5</sup>P. C. Kelires, M. Gioti, and S. Logothetidis, Phys. Rev. B **59**, 5074 (1999).
- <sup>6</sup>D. Wan and K. Komvopoulos, J. Appl. Phys. **100**, 63307 (2006).
- <sup>7</sup>D. Wan and K. Komvopoulos, Appl. Phys. Lett. **88**, 221908 (2006).
- <sup>8</sup>D. Wan and K. Komvopoulos, J. Phys. Chem. C **111**, 9891 (2007).
- <sup>9</sup>Y. Lifshitz, S. R. Kasi, J. W. Rabalais, and W. Eckstein, Phys. Rev. B **41**, 10468 (1990).
- <sup>10</sup>Y. Lifshitz, C. D. Roux, K. Boyd, W. Eckstein, and J. W. Rabalais, Nucl. Instrum. Methods Phys. Res. B **83**, 351 (1993).
- <sup>11</sup>Y. Lifshitz, G. D. Lempert, and E. Grossman, Phys. Rev. Lett. **72**, 2753 (1994).
- <sup>12</sup>R. G. Lacerda, P. Hammer, C. M. Lepienski, F. Alvarez, and F. C. Marques, J. Vac. Sci. Technol. A **19**, 971 (2001).
- <sup>13</sup>S. Asienberg and R. Chabot, J. Appl. Phys. **42**, 2953 (1971).
- <sup>14</sup>J. Ishikawa, Y. Takeiri, K. Ogawa and T. Takagi, J. Appl. Phys. **61**, 2509 (1987).
- <sup>15</sup>P. Kovarik, E. B. D. Bourdon and R. H. Prince, Phys. Rev. B **48**, 12123 (1993).
- <sup>16</sup>B. Petereit, P. Siemroth, H.-H. Schneider, and H. Hilgers, Surf. Coat. Technol. **174-175**, 648 (2003).
- <sup>17</sup>H. Han, F. Ryan, and M. McClure, Surf. Coat. Technol. **120-121**, 579 (1999).
- <sup>18</sup>B. Bhushan, Diamond Relat. Mater. **8**, 1985 (1999).

- <sup>19</sup>S. Anders, A. Anders, I. G. Brown, B. Wei, K. Komvopoulos, J. W. Ager III, and K. M. Yu, Surf. Coat. Technol. **68-69**, 388 (1994).
- <sup>20</sup>D. Liu, G. Benstetter, E. Lodermeier, X. Chen, J. Ding, Y. Liu, J. Zhang, and T. Ma, Diamond Relat. Mater. **12**, 1594 (2003).
- <sup>21</sup>G. M. Pharr, D. L. Callahan, S. D. McAdams, T. Y. Tsui, S. Anders, A. Anders, J. W. Ager III, I. G. Brown, C. S. Bhatia, S. R. P. Silva, and J. Robertson, Appl. Phys. Lett. **68**, 779 (1996).
- <sup>22</sup>P. R. Goglia, J. Berkowitz, J. Hoehn, A. Xidis, and L. Stover, Diamond Relat. Mater. **10**, 271 (2001).
- <sup>23</sup>T. A. Friedmann, J. P. Sullivan, J. A. Knapp, D. R. Tallant, D. M. Follstaedt, D. L. Medlin, and P. B. Mirkarimi, Appl. Phys. Lett. **71**, 3820 (1997).
- <sup>24</sup>B. Schultrich, H.-J. Scheibe, D. Drescher, and H. Ziegele, Surf. Coat. Technol. **98**, 1097 (1998).
- <sup>25</sup>A. Anders, Surf. Coat. Technol. **93**, 158 (1997).
- <sup>26</sup>B. F. Coll, P. Sathrum, R. Aharonov, and M. A. Tamor, Thin Solid Films **209**, 165 (1992).
- <sup>27</sup>A. Anders, Surf. Coat. Technol. **120-121**, 319 (1999).
- <sup>28</sup>A. Anders and R.A. MacGill, Surf. Coat. Technol. **133-134**, 96 (2000).
- <sup>29</sup>G. F. You, B. K. Tay, S. P. Lau, D. H. C. Chua, and W. I. Milne, Surf. Coat. Technol. **150**, 50 (2002).
- <sup>30</sup>T. Schuelke, T. Witke, H.-J. Scheibe, P. Siemroth, B. Schultrich, O. Zimmer, and J. Vetter, Surf. Coat. Technol. **120-121**, 226 (1999).
- <sup>31</sup>K. H. Müller, Surf. Sci. **184**, L375 (1987).
- <sup>32</sup>M. T. Robinson and I. M. Torrens, Phys. Rev. B **9**, 5008 (1974).
- <sup>33</sup>O. S. Oen, D. K. Holmes, and M. T. Robinson, J. Appl. Phys. **34**, 302 (1963).
- <sup>34</sup>M. T. Robinson and O. S. Oen, Phys. Rev. **132**, 2385 (1963).

- <sup>35</sup>W. D. Wilson, L. G. Haggmark, and J. P. Biersack, *Phys. Rev. B* **15**, 2458 (1977).
- <sup>36</sup>J. Lindhard and M. Scharff, *Phys. Rev.* **124**, 128 (1961).
- <sup>37</sup>J. P. Biersack and W. Eckstein, *Appl. Phys. A* **34**, 73 (1984).
- <sup>38</sup>W. Möller and W. Eckstein, *Nucl. Instrum. Methods Phys. Res. B* **2**, 814 (1984).
- <sup>39</sup>O. Vancauwenberghe, N. Herbots, and O. C. Hellman, *J. Vac. Sci. Technol. B* **9**, 2027 (1991).
- <sup>40</sup>J. Biersack, *Nucl. Instrum. Methods Phys. Res. B* **153**, 398 (1999).
- <sup>41</sup>R. Kosiba and G. Ecke, *Nucl. Instrum. Methods Phys. Res. B* **187**, 36 (2002).
- <sup>42</sup>G. Ecke, R. Kosiba, V. Kharlamov, Y. Trushin, and J. Pezoldt, *Nucl. Instrum. Methods Phys. Res. B* **196**, 39 (2002).
- <sup>43</sup>R. M. Hausner, H. Baumann, and K. Bethge, *Nucl. Instrum. Methods Phys. Res. B* **133**, 176 (1996).
- <sup>44</sup>V. S. Veerasamy, G. A. J. Amaratunga, W. I. Milne, J. Robertson, and P. J. Fallon, *J. Non-Cryst. Solids* **164-166**, 1111 (1993).
- <sup>45</sup>E. Byon and A. Anders, *J. Appl. Phys.* **93**, 1899 (2003).
- <sup>46</sup>H. S. Zhang and K. Komvopoulos, *Rev. Sci. Instr.* **79**, 073905 (2008).
- <sup>47</sup>W. Lu and K. Komvopoulos, *J. Tribol.* **123**, 641 (2001).
- <sup>48</sup>M. F. Toney and S. Brennan, *J. Appl. Phys.* **66**, 1861 (1989).
- <sup>49</sup>A. C. Ferrari, A. Libassi, B. K. Tanner, V. Stolojan, J. Yuan, L. M. Brown, S. E. Rodil, B. Kleinsorge, and J. Robertson, *Phys. Rev. B* **62**, 11089 (2000).
- <sup>50</sup>W. Lu, K. Komvopoulos, P. Patsalas, C. Charitidis, M. Gioti, and S. Logothetidis, *Surf. Coat. Technol.* **168**, 12 (2003).
- <sup>51</sup>F. Bridou and B. Pardo, *J. X-ray Sci. Technol.* **4**, 200 (1994).

- <sup>52</sup>F. Bridou, J. Gautier, F. Delmotte, M.-F. Ravet, O. Durand, and M. Modreanu, *Appl. Surf. Sci.* **253**, 12 (2006).
- <sup>53</sup>D. A. Shirley, *Phys. Rev. B* **5**, 4709 (1972).
- <sup>54</sup>S. T. Jackson and R. G. Nuzzo, *Appl. Surf. Sci.* **90**, 195 (1995).
- <sup>55</sup>J. Diaz, G. Paolicelli, S. Ferrer, and F. Comin, *Phys. Rev. B* **54**, 8064 (1996).
- <sup>56</sup>D. R. McKenzie, D. Muller and B. A. Pailthorpe, *Phys. Rev. Lett.* **67**, 773 (1991).
- <sup>57</sup>J. Schwan, S. Ulrich, T. Theel, H. Roth, H. Ehrhardt, P. Becker, and S. R. P. Silva, *J. Appl. Phys.* **82**, 6024 (1997).
- <sup>58</sup>C. A. Davis, K. M. Knowles, and G. A. J. Amaratunga, *Surf. Coat. Technol.* **76-77**, 316 (1995).
- <sup>59</sup>W. Jiang, Y. Zhang, M. H. Engelhard, W. J. Weber, G. J. Exarhos, J Lian, and R. C. Ewing, , *J. Appl. Phys.* **101**, 023524 (2007).
- <sup>60</sup>T. N. Taylor, *J. Mater. Res.* **4**, 189 (1989).
- <sup>61</sup>A. Mahmood, S. Muhl, R. Machorro, A. Lousa, J. Esteve, and J. Heiras, *Diamond Relat. Mater.* **15**, 71 (2006).
- <sup>62</sup>D. Liu, G. Benstetter, and E. Lodermeier, *Thin Solid Films* **436**, 244 (2003).
- <sup>63</sup>D. Wan and K. Komvopoulos, *J. Mater. Res.* **19**, 2131 (2004).

## List of Figures

FIG. 1. Carbon depth profiles simulated with the T-DYN code for 120 eV kinetic energy of carbon ions impinging perpendicular to a silicon substrate surface.

FIG. 2. Carbon depth profiles simulated with the T-DYN code for 20–320 eV kinetic energy of carbon ions impinging perpendicular to a silicon substrate surface and carbon ion fluence equal to (a)  $3.6 \times 10^{16}$  and (b)  $1.8 \times 10^{16}$  ions/cm<sup>2</sup> corresponding to 0.4 and 0.2 min process time.

FIG. 3. XRR results for 0.2–3 min process time, ~120 eV carbon ion kinetic energy (–100 V bias voltage of 25 kHz frequency) and  $\sim 1.48 \times 10^{15}$  ions/cm<sup>2</sup>·s ion flux.

FIG. 4. C1s XPS spectrum of C1s core level peak for ~170 eV carbon ion kinetic energy (–150 V bias voltage of 25 kHz frequency) and 0.4 min process time ( $3.6 \times 10^{16}$  ions/cm<sup>2</sup> ion fluence). The spectrum was fitted by six Gaussian curves after inelastic background subtraction.

FIG. 5. (a) Binding energies of characteristic Gaussian fits of C1s core level peak and (b) fraction of carbon constituents of deconvoluted C1s core level peak vs process time for ~120 eV carbon ion kinetic energy (–100 V bias voltage of 25 kHz frequency).

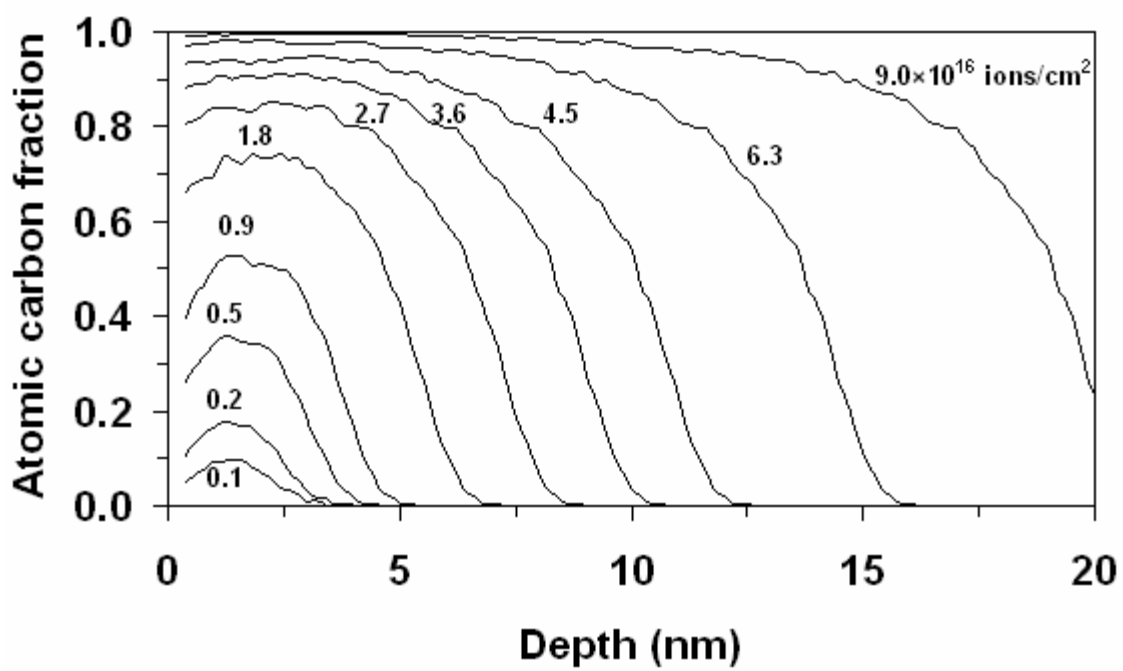
FIG. 6. Carbon constituents of deconvoluted C1s core level peak vs substrate bias voltage of 25 kHz frequency for (a) 0.4 and (b) 0.2 min process time corresponding to  $3.6$  and  $1.8 \times 10^{16}$  ions/cm<sup>2</sup> ion fluence.

FIG. 7. (a) Surface roughness vs process time for ~120 eV ion kinetic energy (–100 V bias voltage of 25 kHz frequency) and (b) surface roughness vs substrate bias voltage of 25 kHz frequency for 0.4 and 0.2 min process time corresponding to  $3.6$  and  $1.8 \times 10^{16}$

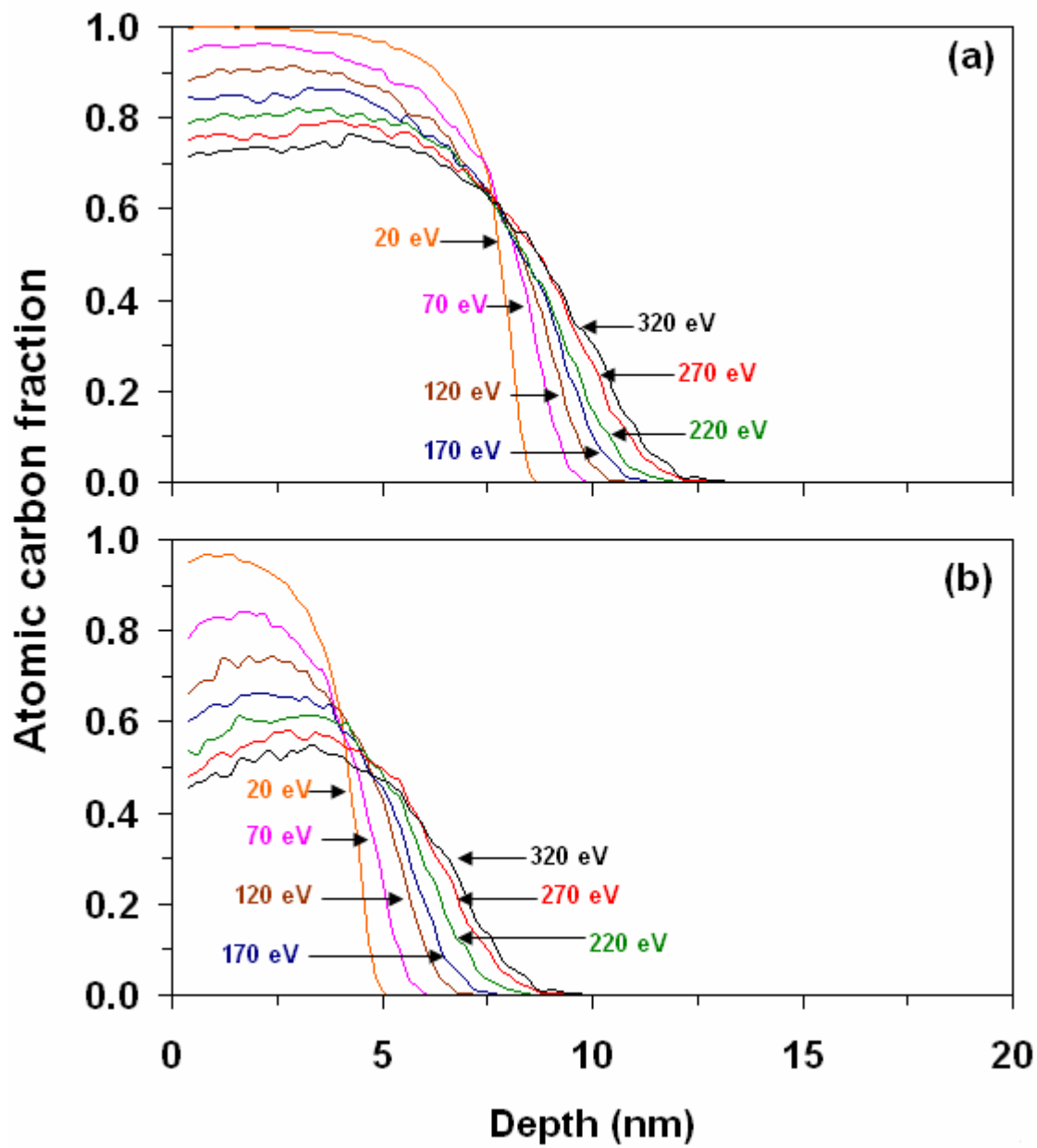
ions/cm<sup>2</sup> ion fluence. The zero-time data point in (a) corresponds to the roughness of the Ar<sup>+</sup> sputter-cleaned Si(100) substrate surface.

FIG. 8. (a) Representative nanoindentation curve and (b) maximum contact pressure vs maximum displacement for a sample processed at ~120 eV ion kinetic energy (−100 V bias voltage of 25 kHz frequency) and 3 min process time.

FIG. 9. (a) Effective hardness vs process time for ~120 eV ion kinetic energy (−100 V bias voltage of 25 kHz frequency), and (b) effective hardness vs substrate bias voltage of 25 kHz frequency for 0.4 and 0.2 min process time corresponding to  $3.6$  and  $1.8 \times 10^{16}$  ions/cm<sup>2</sup> ion fluence.



**Figure 1**



**Figure 2**

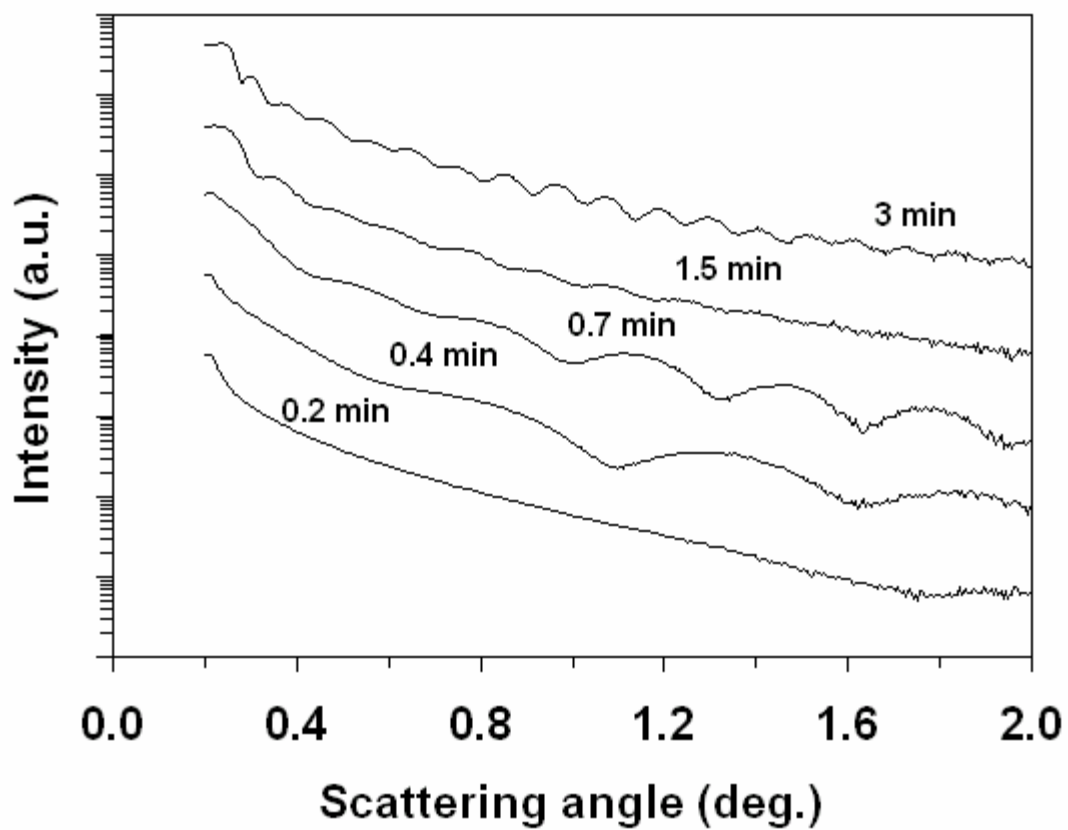


**Figure 3**

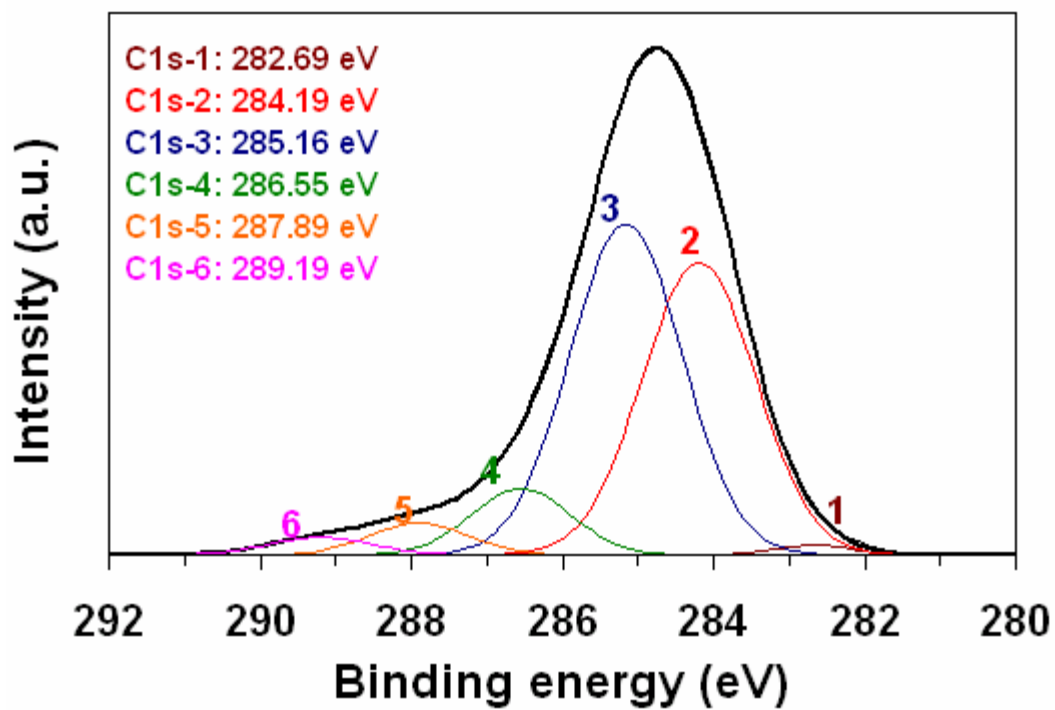


**Figure 4**

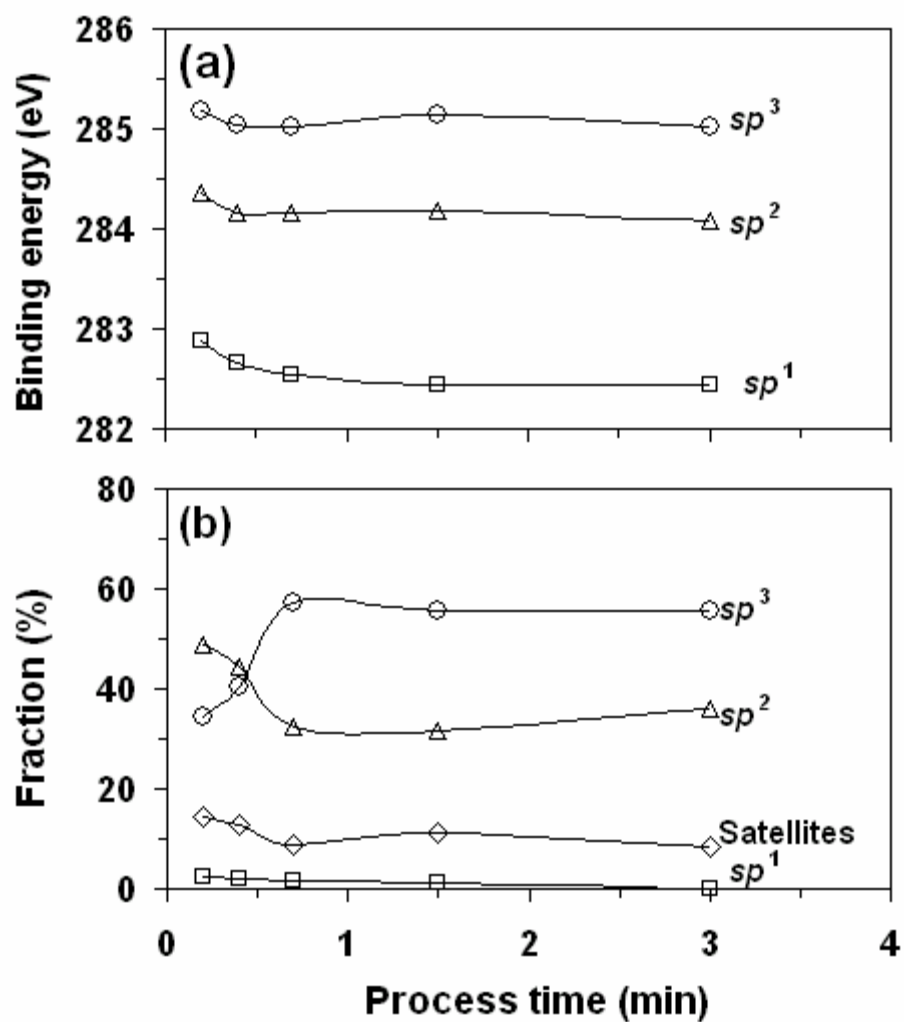
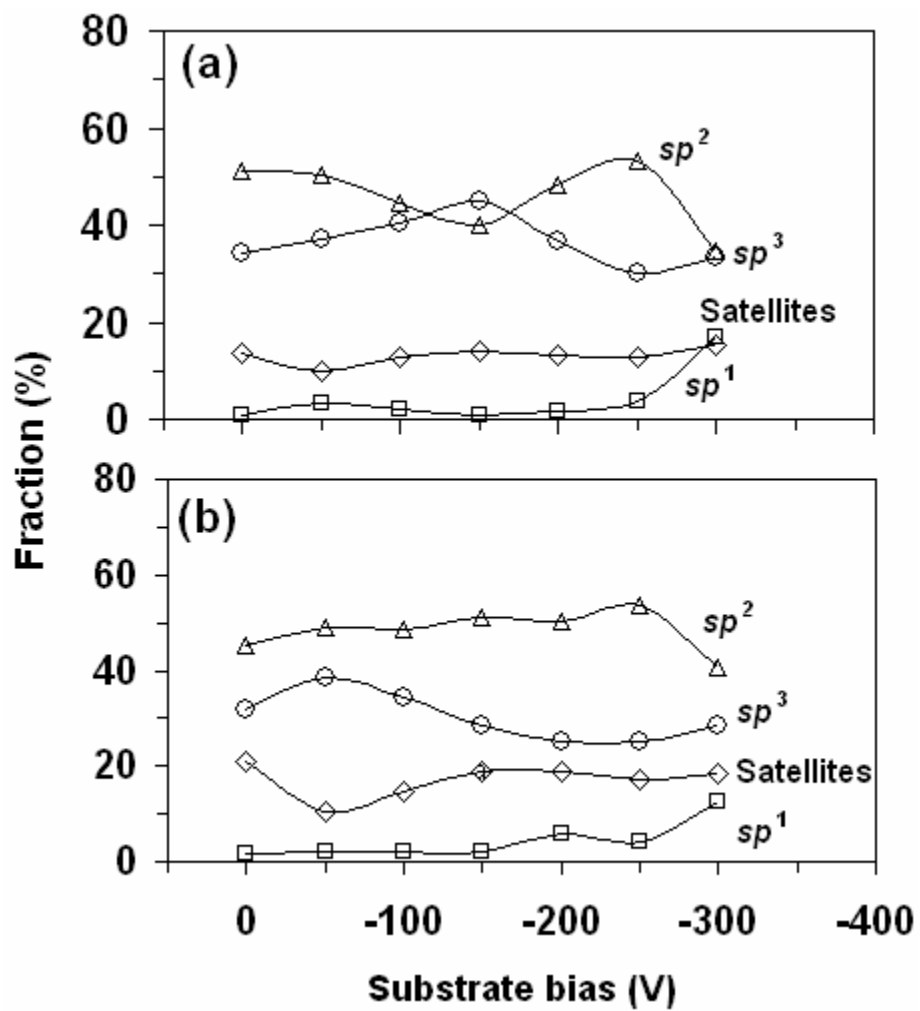
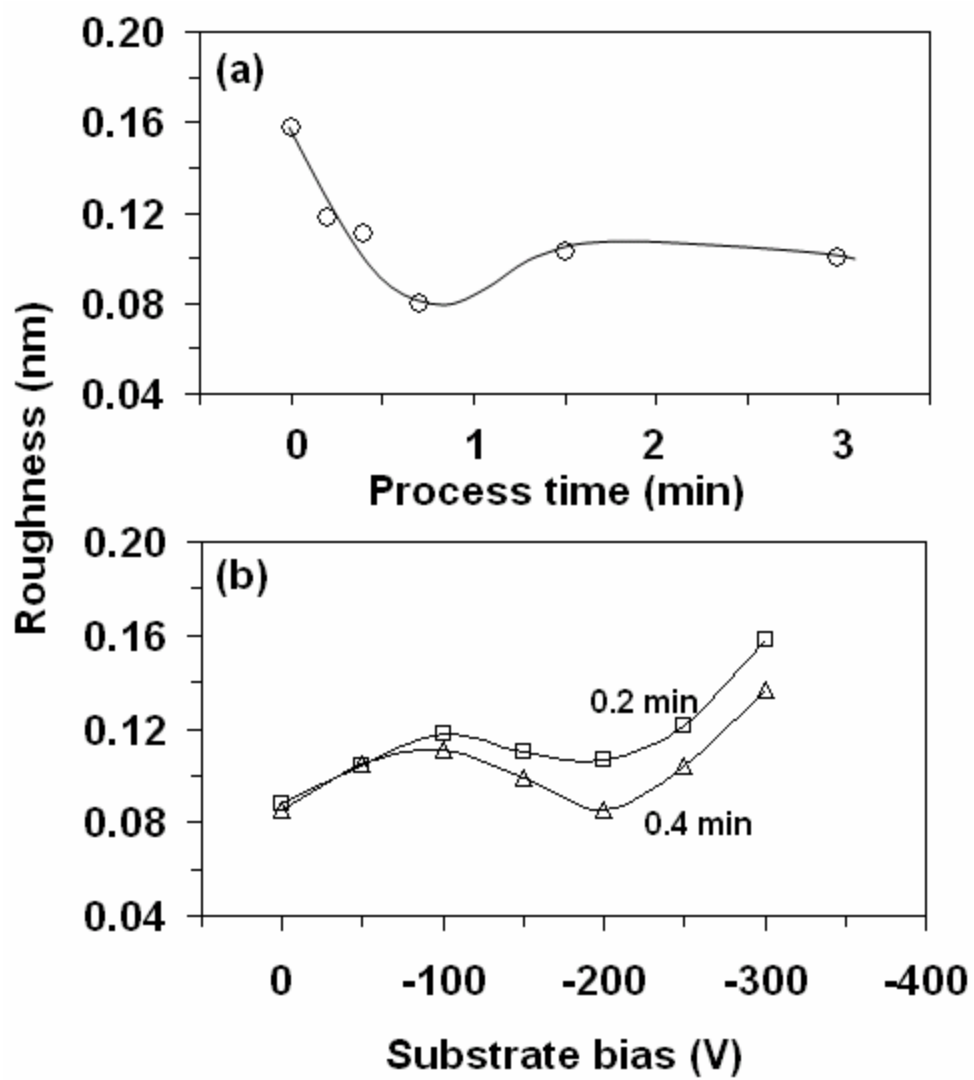


Figure 5



**Figure 6**



**Figure 7**

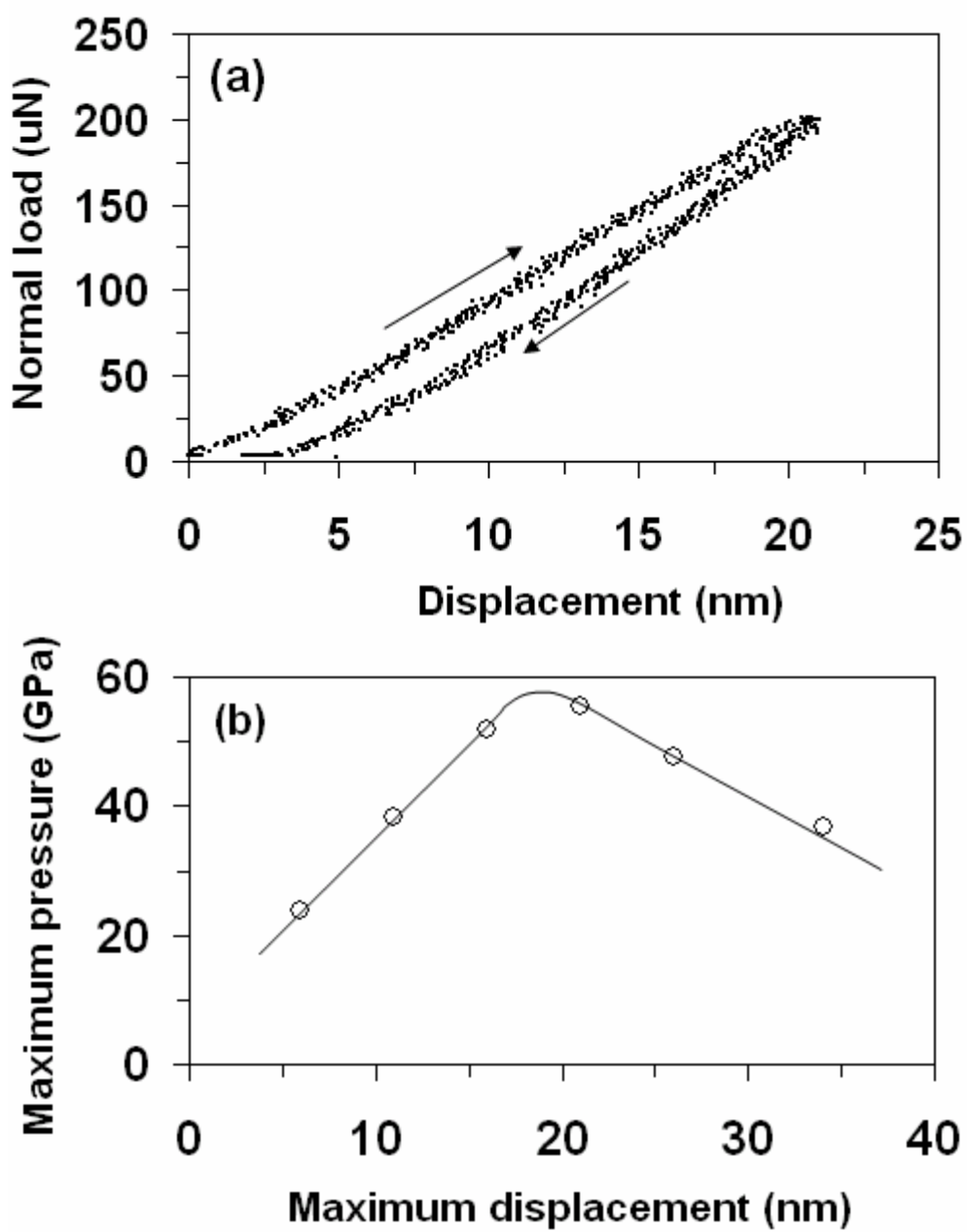


**Figure 8**

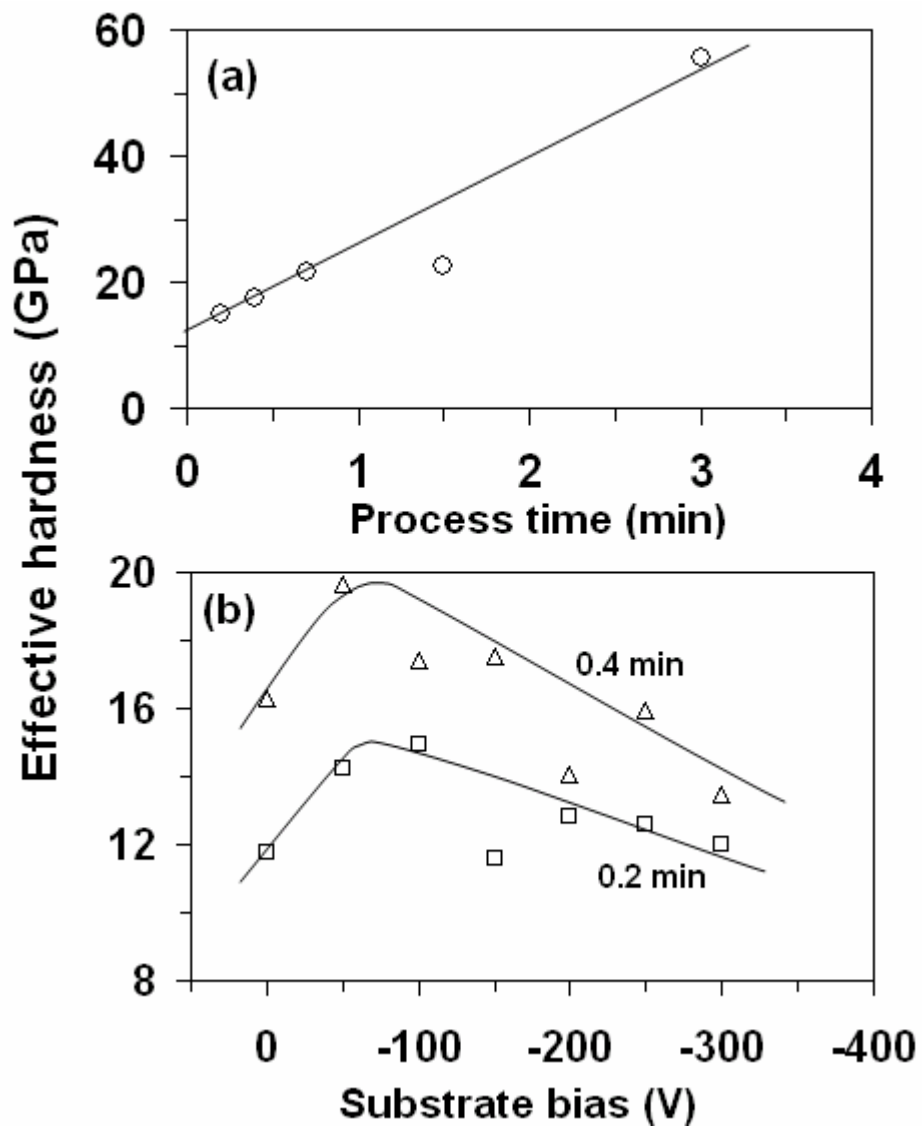


**Figure 9**